Nanoscale

PAPER

View Article Online
View Journal | View Issue

Cite this: *Nanoscale*, 2015, **7**, 3694

Growth and spectroscopic characterization of monolayer and few-layer hexagonal boron nitride on metal substrates

Boris N. Feigelson,*[a] Victor M. Bermudez,[a] Jennifer K. Hite,[a] Zachary R. Robinson,[a,b] Virginia D. Wheeler,[a] Karthik Sridhara[a,c] and Sandra C. Hernández[a]

Received 22nd September 2014,
Accepted 14th January 2015

DOI: 10.1039/c4nr05557h

www.rsc.org/nanoscale

Atomically thin two dimensional hexagonal boron nitride (2D h-BN) is one of the key materials in the development of new van der Waals heterostructures due to its outstanding properties including an atomically smooth surface, high thermal conductivity, high mechanical strength, chemical inertness and high electrical resistance. The development of 2D h-BN growth is still in the early stages and largely depends on rapid and accurate characterization of the grown monolayer or few layers h-BN films. This paper demonstrates a new approach to characterizing monolayer h-BN films directly on metal substrates by grazing-incidence infrared reflection absorption spectroscopy (IRRAS). Using h-BN films grown by atmospheric-pressure chemical vapor deposition on Cu and Ni substrates, two new sub-bands are found for the A_{2u} out-of-plane stretching mode. It is shown, using both experimental and computational methods, that the lower-energy sub-band is related to 2D h-BN coupled with substrate, while the higher energy sub-band is related to decoupled (or free-standing) 2D h-BN. It is further shown that this newly-observed fine structure in the A_{2u} mode can be used to assess, quickly and easily, the homogeneity of the h-BN–metal interface and the effects of metal surface contamination on adhesion of the layer.

Introduction

Since graphene has become a material of choice for many advanced electronic and optoelectronic applications,[1] single-crystal 2D h-BN (two dimensional hexagonal boron nitride) has also drawn serious attention as the most suitable substrate for maintaining the exceptional transport properties of graphene.[2,3] Boron nitride is a remarkable material with unique physical and chemical properties, which also is a fascinating structural analogue of carbon.[4] Graphite-like h-BN is an insulator with a large bandgap of 5.9 eV,[5,6] an atomically smooth surface that is expected to be free of dangling bonds and charge traps,[2] and a lattice constant similar to that of graphite. In addition, h-BN possesses a thermal conductivity comparable to that of graphene.[6,7]

It is this unique combination of properties that makes h-BN an appealing substrate for graphene in electronic applications. Furthermore, 2D h-BN is also a critical element for the development of new types of tunneling devices based on graphene/h-BN heterostructures[8] or, more generally, as a key part of 2D-based van der Waals heterostructures.[9] One layer or a multilayer of h-BN can be mechanically exfoliated from bulk single crystal h-BN in the same manner as graphene, and can be stacked vertically with other materials to develop 2D heterostructures.[8] However, for industrial applications, large-area 2D h-BN is required. It has been shown that h-BN can be grown on metallic substrates by chemical vapor deposition (CVD)[10,11] and that solid ammonia borane (NH_3–BH_3) can be used as a precursor for atmospheric-pressure CVD h-BN growth.[12,13] The CVD growth of 2D h-BN is a compelling approach for the future development of 2D van der Waals heterostructures; however, this process substantially depends on rapid and accurate characterization of the grown films.

It is known that phonon spectra can give useful information about the structural quality of the 2D h-BN film, its thickness, its interaction with a substrate and the possible buckling of the BN monolayers.[14] Raman- and infrared (IR)-active vibrational modes in h-BN have been intensively investigated,[14,15] and the corresponding spectra can be considered as convenient tools for 2D materials characterization. Graphene is a good example, demonstrating the power of vibrational Raman spectroscopy in studying and characterizing a 2D material even directly on a metal substrate after growth.[16]

[a]*U.S. Naval Research Laboratory, 4555 Overlook Ave., SW, Washington, DC 20375, USA. E-mail: boris.feygelson@nrl.navy.mil*
[b]*ASEE Postdoctoral Fellow residing at U.S. Naval Research Laboratory, 4555 Overlook Ave., SW, Washington, DC 20375, USA*
[c]*Department of Material Science and Engineering, University of Maryland, College Park, MD 20742, USA*

Unfortunately, the characteristic Raman-active E_{2g} mode of a single layer of h-BN, located at ~1366 cm^{-1}, is about 50 times weaker than the analogous G peak of graphene.[17] This makes Raman spectroscopy an inefficient tool for the characterization of thin 2D h-BN films directly on metal substrates. Thin h-BN films on a metal substrate also cannot be characterized, using IR transmission spectra, which requires transfer of the film to an IR-transparent substrate.

One of the possible approaches to consider for 2D h-BN characterization is grazing-incidence infrared reflection absorption spectroscopy (IRRAS) which is used to analyze very thin coatings on metal substrates.[18,19] An important feature of this technique is that the incident beam is polarized in the plane of incidence since only *p*-polarized radiation exhibits sensitivity to thin films on metallic surfaces.[18,19] The reflected *p*-polarized light provides information on IR absorption by a few nanometer thick film on a metal surface.

In this work, the IR-active out-of-plane vibrational mode of 2D h-BN films grown by atmospheric-pressure CVD on metal substrates (mainly Cu but also Ni) is exploited to identify 2D h-BN directly on substrates and studied both computationally and experimentally. It is found that the mode energy depends sensitively on the strength of the interaction between the layer and the substrate and that doublet structure in this mode, reported here for the first time, can be used to assess quickly and easily the film coverage and the degree of interaction at the BN–metal interface. The essential purpose is to show how IR reflectance spectroscopy can be used to characterize the interaction between BN and a metallic substrate and also to rationalize the small sample-dependent differences in the exact BN mode frequency. In the process of pursuing this objective we have gained insight into the effects of sample aging and of chemical treatment of the substrate on the strength of the interaction. Subsequent studies will relate these results to the growth of large-area BN films and will investigate on a more fundamental level the surface science of the BN-substrate interaction.

Experimental

A vertical custom-made CVD reactor was used to grow 2D h-BN on metal substrates at atmospheric pressure. The design of the vertical reactor allows the simultaneous growth of a few samples of h-BN or graphene on different substrates in the same run. The schematic of the reactor is shown in Fig. 1.

Copper foil (Alfa Aesar 99.999%, 25 μm), single crystal Cu (MTI Corporation 99.9999%, 10 × 10 × 0.5 mm), and polycrystalline Ni (MTI Corporation >99.9%, 10 × 10 × 0.5 mm) were used as substrates. All substrates were sonicated for 5 min in acetone and 5 min in isopropyl alcohol before loading in the reactor. Copper foil substrates were initially pressed in an MTI 12 T hydraulic press between two hard steel anvils under a pressure of about 0.35 GPa to cause plastic deformation. Prior to growth, the Cu foil was annealed in Furnace 1 under a flow of 180 standard cm^3 min^{-1} (sccm) of N_2 and 20 sccm of H_2 for

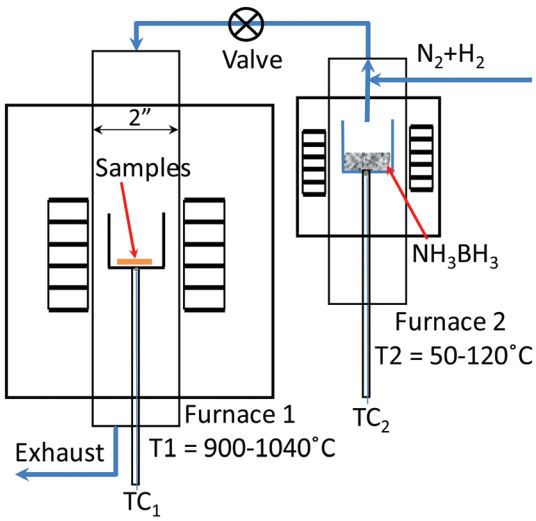

Fig. 1 Schematic view of the vertical CVD reactor for 2D h-BN growth.

4 hours at the growth temperature. Ammonia borane (NH_3–BH_3) from BoroScience International, Inc. (99.9% purity) was used as the precursor for boron nitride growth.[12] It was sublimed in Furnace 2 at temperatures of 60–90 °C and transported by a carrier gas mixture of 840 sccm of N_2 and 20 sccm of H_2 to the Furnace 1 reactor. Boron nitride was grown on Cu or Ni substrates at temperatures of 930 °C or 1030 °C as measured by a thermocouple directly at the bottom of the crucible. After h-BN growth the flow of carrier gas was redirected to Furnace 1, which then was cooled down to room temperature (RT) under the flow of N_2 + H_2. All samples after growth were examined by optical microscopy using both a Motic SMZ-168TL Stereo Microscope and an Olympus BH-2 Microscope with Nomarski contrast. Surface morphology on a finer scale was also studied by scanning electron microscopy (SEM) using a LEO Supra 55 microscope. By examining the SEM images, growth features and film coverage of the sample can be determined.

X-ray photoelectron spectroscopy (XPS) was performed on a series of samples to analyze the impact of growth parameters on the chemical structure and thickness of the resulting films. Following growth, the samples were transferred through air from the growth chamber to the XPS chamber. All spectra were collected using a Thermo-Scientific K-Alpha spectrometer with a monochromatic Al-Kα source (1486.6 eV) positioned at 53.5° with respect to the sample normal and a spot size of 0.4 mm. A 128 channel hemispherical electron energy analyzer was used to measure the energy of the photoelectrons with a takeoff angle parallel to the sample normal. Binding energies (BEs) were calibrated using the Au $4f_{7/2}$ (BE = 84.0 eV) and adventitious carbon C 1s (BE = 284.9 eV) peaks. Low-resolution survey spectra were acquired using a pass energy of 200 eV with 1 eV step size, while high-resolution core level scans were collected using a pass energy of 20 eV and steps of 0.15 eV.

Fourier transform (FT) IRRAS spectra were recorded using a Thermo Scientific Nicolet 8700 spectrometer combined with a

Harrick Scientific Products "Focus" grazing-angle reflection accessory. The angle of incidence was 75°, and all spectra were recorded in *p*-polarization. A liquid-N_2-cooled wide-band HgCdTe (MCT-B) detector was used, and 1000 scans at 4 cm^{-1} resolution were averaged over about 10 min. Data are presented in the form of absorbance = $-\log_{10}(R_1/R_0) \approx (\delta R/R_0)/2.303$ where R_0 is the reflectance spectrum of the bare metal substrate, and $R_1 = R_0 + \delta R$ is the reflectance with the BN layer added. The quantity $\delta R/R_0$ is then the fractional change in reflectance due to the BN layer, which can be related directly to the BN absorption spectrum.[18] The same bare-Cu foil was used to record R_0 for all data sets, but each h-BN sample was grown on a different foil piece. Hence, in addition to the h-BN A_{2u} mode (which is always reproducible), $(\delta R/R_0)$ also shows spurious and non-reproducible structure due to differences between the two Cu foils with regard to flatness, surface texture and contamination, degree of crystallinity, *etc*.

Computational

Ab initio calculations using density functional theory (DFT) were performed in order to assess the effect of the Cu substrate on the out-of-plane vibrational mode of an h-BN monolayer. The *Quantum Espresso* (vers. 5.0)[20] code was used with ultrasoft pseudopotentials and energy and density cutoffs of 60 and 720 Rydberg respectively, together with the Perdew-Burke-Ernzerhof functional modified for solid-state applications (PBEsol). In geometry optimization the convergence criteria were 2.6 meV $Å^{-1}$ for the maximum force on any atom and 0.14 meV for the change in total energy. Monkhorst-Pack grids of 16 × 16 × 16 and 16 × 16 × 6 were used for bulk Cu and h-BN respectively while a 16 × 16 × 1 grid was used for two-dimensionally-periodic (2DP) slab calculations. For comparison, some calculations (termed "PBE_{sol} + D2") were also done with inclusion of the Grimme D2 semi-empirical dispersion correction.[21] The adsorption energy for the h-BN layer on the Cu substrate is given by $\Delta E_{ads} = E(\text{Cu + BN}) - [E(\text{Cu}) + E(\text{BN})]$ where the first term is the relaxed total energy of h-BN/Cu, and the others are those of the separated components (also relaxed). Since $E < 0$, a negative ΔE_{ads} indicates an exothermic interaction. All calculations involving Cu were spin-unrestricted (since the Cu atom has an odd number of electrons) but converged to a non-magnetic configuration.

Results and discussion

Annealing a plastically-deformed Cu foil resulted in an average grain size of a few mm^2, which is substantially larger than that of a foil that was annealed without prior deformation. This is illustrated in the images of the unpressed and annealed Cu foils in Fig. 2a and b *versus* those of pressed and annealed foils in Fig. 2c and d. Fig. 2a and c are optical micrographs while Fig. 2b and d are Nomarski images at a larger magnification. The driving force for such grain growth during annealing is the reduction of stored energy, *via* a reduction in grain boundary surface area,[22] but specific mechanisms of the observed growth require further investigation. From these Nomarski images, it is shown that the surface of a pressed Cu foil after annealing is also smoother in comparison with its unpressed counterpart. It is expected that the larger average grain size, the uniform crystallographic orientation and the smoother surface exhibited by a pressed and annealed substrate will all be beneficial for uniform h-BN growth.

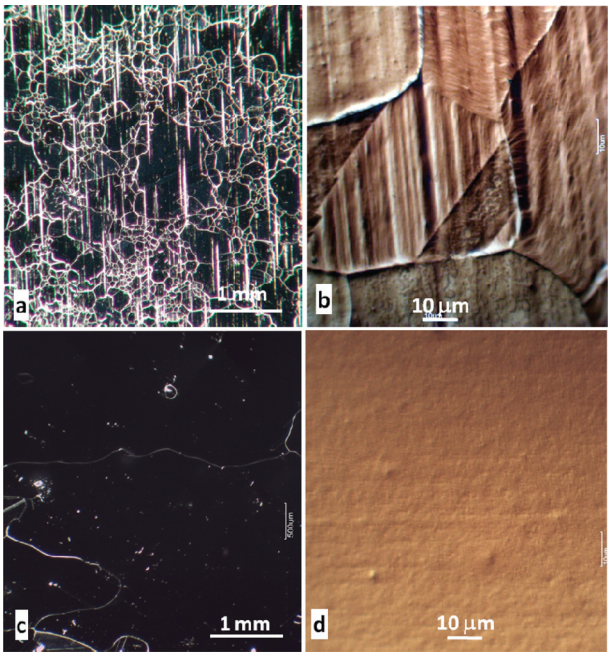

Fig. 2 (a) is an optical micrograph of an upressed Cu-foil after annealing; (b) is a Nomarski image of the same foil; (c) is an optical micrograph of a pressed foil alter annealing and (d) is a Nomarski image of the same foil.

Survey XPS spectra after h-BN growth verified the presence of BN on all Cu foils (Fig. 3a). Examples of high resolution B 1s and N 1s core level spectra can be seen in Fig. 3b and c, respectively. The single B 1s peak at 190.5 eV and N 1s peak at 398.2 eV correspond to BN with no evidence (in the form of satellite structure) of any impurity incorporation.[23] However, in the survey spectra, small amounts of both oxygen and carbon impurities are still observed. High resolution spectra of

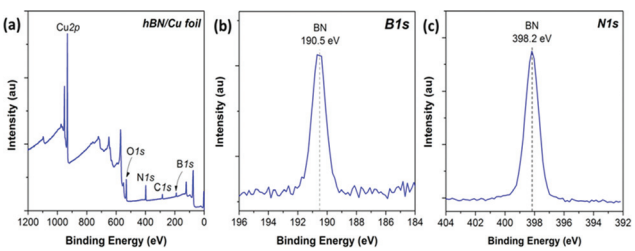

Fig. 3 XPS spectra from a representative sample of h-BN on Cu foil. (a) Survey spectrum used to identify the elements present; (b) and (c) high resolution B 1s and N 1s peaks corresponding to the BN film.

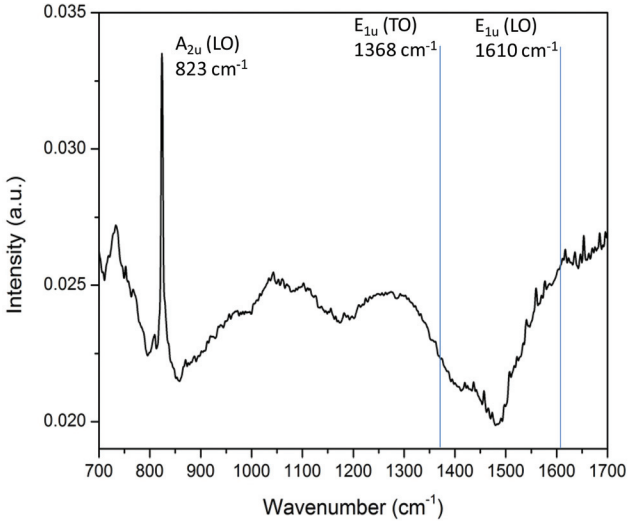

Fig. 4 Typical FT-IRRAS data for a 2D h-BN film on Cu. E_{1u} (TO)" and "E_{1u} (LO)" mark the positions where these modes would be seen if they were detectable in the present experiments. The intensity is in absorbance units (a.u.).

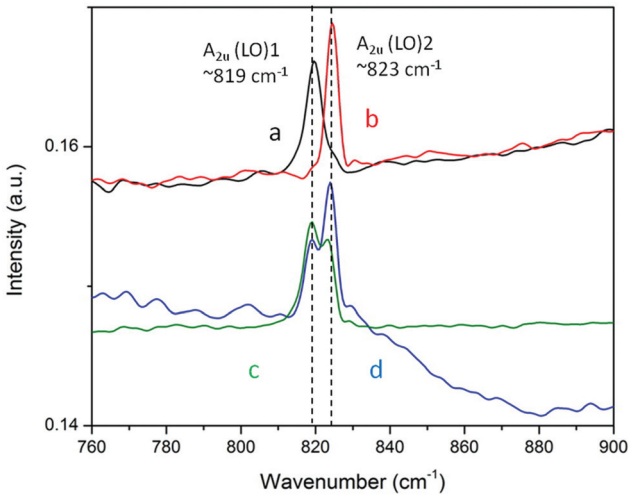

Fig. 5 Representative spectra of different alternatives found within FT-IRRAS of 2D h-BN film on Cu for A_{2u} (LO) vibration with two sub-bands: A_{2u}(LO)1 and $A_{2u}(LO)_2$.

the C1s and O1s peaks (not shown) reveal that these result from various C–O and C═O species, which are most likely absorbed during transfer to the XPS chamber. There is typically a small oxide peak (not shown) associated with the Cu $2p_{3/2}$, which most likely results from oxidation of exposed Cu on samples with incomplete h-BN growth.

A typical FT-IRRAS spectrum of h-BN on Cu foil is shown in Fig. 4. Only the out-of-plane A_{2u} (LO) vibrational mode, giving the peak at 823 cm^{-1} (ref. 24), is observed. There are no detectable peaks due to the in-plane 1368 cm^{-1} E_{1u} (TO) and 1610 cm^{-1} E_{1u} (LO) vibrations.[24] In a grazing-incidence, *p*-polarized reflection experiment one would expect the absence of these peaks for a very thin 2D h-BN film on a metallic substrate.[18,19] The other structure in Fig. 4 represents the spurious baseline artifacts discussed in the Experimental section.

Careful investigation of numerous different 2D h-BN films on Cu foils revealed more complex structure in the FT-IRRAS data. It was found that two prominent peaks corresponding to the A_{2u}(LO) mode can be observed in these spectra: A_{2u}(LO)1 at around 819 cm^{-1}, shown in Fig. 5 by the black plot (a), and A_{2u}(LO)2 at around 823 cm^{-1}, shown by the red plot (b). Spectra with both peaks present simultaneously and with different relative intensity of these peaks shown by green (c) and blue (d) plots, respectively, were also observed. Only these two types of peaks were found for any of the samples.

Initial FT-IRRAS experiments with h-BN successfully demonstrated the potential of this technique to conveniently characterize 2D h-BN directly on a Cu substrate. Nevertheless, the discovery of two sub-bands associated with the A_{2u}(LO) mode, with varying relative intensity, required in-depth interpretation. In the beginning, in order to correlate the intensity of the A_{2u}(LO) peaks and the properties of the h-BN films, 2D h-BN layers of different coverage and thickness were grown in a series of runs. Following these growth runs, XPS and FT-IRRAS, along with SEM imaging, were performed on each of the samples.

The thickness of the h-BN cannot easily be obtained from the IR intensity. By calculating the area under the B 1s XPS peak for each sample and comparing it with the area under the Cu $2p_{3/2}$ peak, an effective h-BN film thickness was obtained according to the commonly used model in ref. 25, 26. This model assumes a uniform attenuating overlayer of thickness d above a flat, semi-infinite substrate. Since the samples may not be perfectly uniform in thickness (*i.e.*, the second h-BN layer may nucleate before the first layer completely coalesces) and the Cu foil may not be perfectly flat, the thickness is referred to as an "effective thickness" and is expected to follow the same trend as the absolute coverage. The effective film thickness was calculated using eqn (1) where I_B and I_{Cu} are the intensities of the B 1s and Cu $2p_{3/2}$ peaks, respectively.

$$\frac{I_B}{I_{Cu}} = \frac{\frac{\rho_{BN}}{M_{BN}}\sigma_B\lambda_1\cos\theta(1-\exp[-d/(\lambda_1\cos\theta)])}{\frac{\rho_{Cu}}{M_{Cu}}\sigma_{Cu}\lambda_2\cos\theta(\exp[-d/(\lambda_3\cos\theta)])} \quad (1)$$

In the numerator, ρ_{BN} is the density of h-BN, M_{BN} is the molecular weight of BN, σ_B is the B 1s photoionization cross-section,[27] λ_1 is the effective attenuation length (EAL) of a B 1s photoelectron in h-BN and θ is the angle between the sample normal and the photoelectron detector. The denominator is similar, except that λ_2 and λ_3 are the EALs of a Cu $2p_{3/2}$ photoelectron in Cu and h-BN, respectively. The EALs of the photoelectrons were calculated using the NIST EAL database.[28] Using this equation, the effective thickness of the h-BN films for several samples of different I_B/I_{Cu} ratios was solved for numerically and compared with FT-IRRAS data taken on the same films. A plot of the area under the FT-IRRAS A_{2u}(LO)

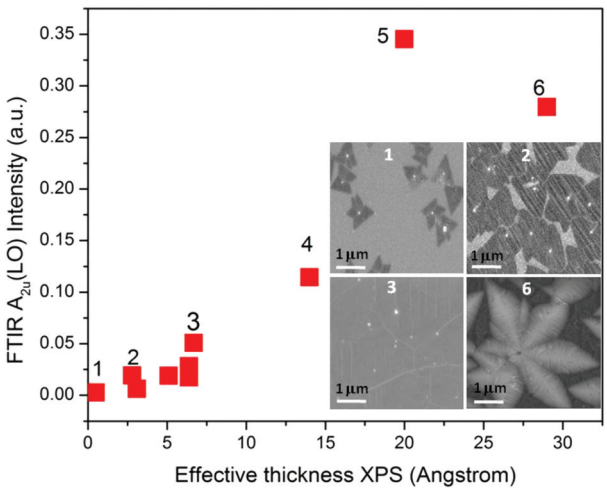

Fig. 6 FT-IRRAS A_{2u}(LO) band intensity *vs.* XPS effective thickness. The FTIR intensities are measured based on the total intensity of the 2 modes at about 819 and about 823, while the thickness measured by XPS was calculated based on the area ratio of the B 1s and Cu 2p peaks. The inset shows SEM images as references of film coverage and morphology.

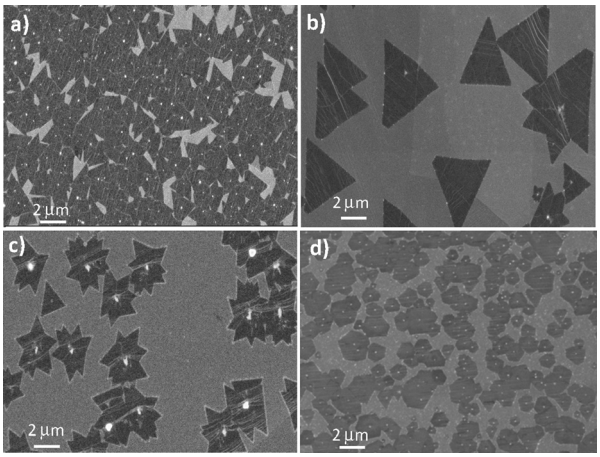

Fig. 7 SEM images of 2D h-BN samples with different crystal sizes, coverage of the Cu substrate and crystal morphology. Such variations in 2D h-BN features do not show any correlation with A_{2u}(LO) peak position: (a) 820.0 cm^{-1}; (b) 822.4 cm^{-1}; (c) 818.5 cm^{-1}; (d) 820.0 cm^{-1}.

peaks *vs.* the effective thickness can be seen in Fig. 6, which shows an essentially-monotonic increase in FT-IRRAS intensity as the effective film thickness increases. The same correlation between amount (effective film thickness) of h-BN and A_{2u}(LO) intensity can be seen when one compares XPS and FT-IRRAS with SEM images of the same samples shown in the inset in Fig. 6, which demonstrates the increase in coverage on the Cu foil up to the full coverage by the 2D h-BN film in sample #3 and by the thick dendritic film in sample #6. A shift of the point 5 from the monotonic pattern can be attributed to the non-uniform h-BN coverage on the polycrystalline Cu substrate and to the substantial difference between areas which are characterized by FT-IRRAS (the whole sample) and by XPS (400 μm). The scatter in the data, which are intended only to indicate a trend, results from the approximate nature (discussed above) of the XPS thickness determination.

An unsystematic comparison was made of many different samples grown under various conditions, which results in different crystal sizes (up to 4 μm), substrate coverages and crystal shapes leading to different edge terminations.[13] This did not reveal any pattern in the nature of the two prominent peaks for the out-of-plane vibration. The appearance of the peaks around 819 cm^{-1} or 823 cm^{-1} seemed to be random without any correlation with the morphological features of the films. Examples shown in Fig. 7a, b, c and d have A_{2u}(LO) peak position at 820.0 cm^{-1}, 822.4 cm^{-1}, 818.5 cm^{-1} and 820.0 cm^{-1} respectively.

To explain the origin of two peaks related to A_{2u}(LO) vibration mode, *ab-initio* calculations were performed in order to assess the effect of the Cu substrate on the vibrational modes of a monolayer of h-BN. The main purpose of the computational work is to support the experimental effort by showing that the interaction between h-BN and a metallic substrate leads to a red-shift in the BN LO phonon, the magnitude of which increases with the strength of the interaction. An ideal model is employed in which a perfectly flat BN layer is in contact with an atomically-clean, smooth and flat Cu (111) substrate.

There have been several previous computational studies[29–32] of h–BN on Cu, but none have dealt with vibrational spectra. The main interest in the present work is in the out-of-plane B–N stretching mode at the Γ-point, which is the only mid-IR mode detectable in the present experiments. As a first step, observed and calculated results were compared for bulk Cu and bulk h-BN, as shown in Table 1. In all cases, comparison of the results of the static calculations is made with experimental values obtained at low temperature ($\lesssim$50 K).

The results are seen to be in reasonable agreement for both materials. The computed Γ-point frequency for the LO branch of the out-of-plane mode in bulk h-BN is 804.4 cm^{-1} *versus* the present experimental value of 824 cm^{-1}. This small discrepancy (~3%) probably arises largely from the use of the harmonic approximation and from errors in the computed high- and

Table 1 Observed and calculated values for lattice constants (a_0, c_0, in Å), cohesive energy (ΔE_c, in eV per Cu atom or per BN unit) and bulk modulus (B_0, in GPa) for bulk Cu and bulk h-BN

		PBEsol	Expt. (Ref.)
Cu	a_0	3.583	3.595 (33)[a]
	ΔE_c	3.95	3.52 (33)
	B_0	168	142 (33)
h-BN	a_0, c_0	2.504, 6.887	2.506, 6.603 (34)
	ΔE_c	14.7	13.4 (35)[b]

[a] Ref. 33 is a computational study that, however, summarizes experimental results from the literature for a wide range of metals. [b] There are, to our knowledge, no experimental results for the ΔE_c of hexagonal BN. The value quoted is from a second-order Møller-Plesset (MP2) calculation,[35] which is *de facto* at T = 0 K and which also reliably treats inter-layer van der Waals interaction.

low-frequency dielectric constants. In this work, only changes in frequency due to BN–Cu interaction, and not absolute values, are of interest. The corresponding computed value for a free-standing BN monolayer is 804.7 cm^{-1}. To model h-BN/Cu, a (111)-oriented 2DP slab with six Cu layers was used as the substrate.

Previous work[36] shows that a 3-layer slab is sufficient to give a converged surface energy for Cu (111). During relaxation, the bottom-most Cu layer was fixed in the optimized bulk configuration while the other five layers, together with the h-BN monolayer, were unconstrained. For a face-centered-cubic (*fcc*) metal such as Cu, calculations of the type described above can be performed only on the (111) surface, since it is necessary for the substrate to be commensurate with the h-BN layer. The Cu–Cu nearest-neighbor distance in the (111) plane is $a_0/\sqrt{2}$, which for PBEsol is 2.534 Å (Table 1) *versus* the computed BN in-plane lattice constant of 2.504 Å. This ~1.2% mismatch was addressed by reducing the Cu lattice constant to match that of BN, thus giving a commensurate structure. The B and N atoms in the h-BN monolayer can lie above a Cu atom (*top*), above a first-underlayer Cu atom in a hexagonally-close-packed (*hcp*) site or above a first-underlayer hollow (*fcc*) site. Previous work[31] indicates that N(*top*) + B(*fcc*) and N(*top*) + B(*hcp*) give very similar ΔE_{ads} values and are more stable than any other structure. In the present work, in order to examine the effects of varying ΔE_{ads}, we will consider N(*top*) + B(*hcp*) and also B(*top*) + N(*hcp*), for which ΔE_{ads} is nearly zero at the PBE_{sol} level. The results are summarized in Table 2.

Compared to experiment,[37] PBE_{sol} underestimates ΔE_{ads}; whereas, PBE_{sol} + D2 overestimates this quantity. For N(*top*) + B(*hcp*) no modes with imaginary frequencies are found for PBE_{sol}, which indicates a stable structure. On the other hand, one imaginary value is found for the less-stable B(*top*) + N(*hcp*), consistent with this structure being a metastable transition state in the displacement of the h-BN layer relative to the substrate. For completeness, results have also been obtained for N(*top*) + B(*hcp*) using PBEsol + D2. For this calculation both bulk Cu and h-BN were also re-optimized using PBE_{sol} + D2. This gives ν(IR) = 758.1 cm^{-1} together with two imaginary frequencies, which is again consistent with the fact that, at the PBEsol + D2 level, this structure is less stable than N(*top*) + B(*fcc*) (by 1.8 meV). The essential point demonstrated by these results is that ν(IR) decreases with increasing ΔE_{ads}. This suggests that the intra-layer B–N bond strength decreases as the bonding of B and/or N to the substrate increases. It is noted that the computed shifts are significantly larger than those seen experimentally. This is a result of the fact that the chemically- and structurally-heterogeneous real h-BN–Cu interface will exhibit a weaker interaction than the ideal interface assumed in the model calculations.

To verify the theoretical predictions and to estimate the effect of the metal substrate on the energy of the A_{2u}(LO) mode, the growth of 2D h-BN on three different Cu single crystal substrates was performed in the same run: Cu(111), Cu(100) and Cu(110) along with a polycrystalline Cu foil. All samples were grown at 930 °C for 30 min. We assume here that, experimentally, the h-BN–Cu interaction will be weaker on Cu surfaces other than (111) due to the lack of registry between the film and the substrate. This is supported by theoretical results for h-BN monolayers on the (111) surfaces of a range of *fcc* metals, which show that the strain energy in the BN layer increases with the degree of lattice mismatch between h-BN and the substrate.[29] SEM images (not shown) indicated that h-BN films on Cu (100), Cu (110) and Cu foil consist primarily of 2D h-BN crystallites while the film on Cu (111) is mostly continuous. The corresponding FT-IRRAS spectra are shown in Fig. 8a.

Growth of four different samples in the same run allowed minimal influence of uncontrolled variations in growth con-

Table 2 Similar to Table 1 but showing computed results for a single h-BN layer on Cu (111). a_0 is the lattice constant and d(X–Cu) the distance (both in Å) between the top Cu layer and X = B or N. N_Z–B_Z is the difference (in Å) between the surface-normal coordinate of B and N, with B always being closer to the Cu surface. ΔE_{ads} is the adsorption energy (in meV per BN). A negative ΔE_{ads} indicates an exothermic (bonding) interaction. ν(IR) is the frequency (in cm^{-1}) of the mid-IR out-of-plane stretching mode. The B(*top*) + N(*hcp*) structure is not stable for PBEsol + D2 and relaxes to N(*top*) + B(*fcc*)

		PBEsol	PBEsol + D2	Expt.[37]
B(*top*) + N(*hcp*)	a_0	2.504		
	d(B–Cu)	3.562		
	N_Z–B_Z	0.005		
	ΔE_{ads}	−4.8		
	ν(IR)	791.6		
N(*top*) + B(*hcp*)	a_0	2.504	2.502	
	d(N–Cu)	3.341	2.838	3.00
	N_Z–B_Z	0.007	0.021	
	ΔE_{ads}	−16.5	−296	−59.7
	ν(IR)	785.4	758.1	

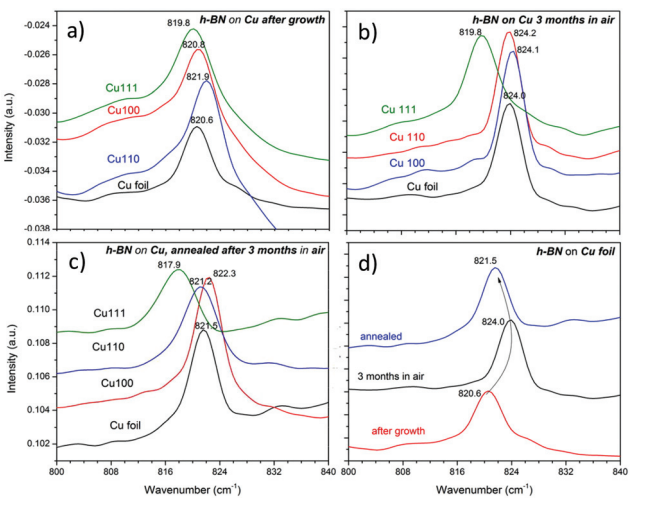

Fig. 8 FT-IRRAS data for four 2D h-BN samples on Cu (111), (100), (110) single crystals and on Cu foil grown simultaneously: (a) as grown; (b) after 3 months storage in air; (c) after annealing in H_2; (d) progression of the A_{2u}(LO) peak position in h-BN grown on Cu foil through all three stages.

ditions on the resulting h-BN films. The A_{2u}(LO) peak of h-BN on Cu (111) is located at 819.8 cm^{-1}, the lowest energy position among all measured peaks in this growth run. In light of the computational results, this suggests that the h-BN–Cu interaction is the strongest in this case. The position of the peak associated with h-BN on Cu foil is somewhere among those on single-crystal substrates of the three different orientations, which is expected since this polycrystalline substrate comprises Cu grains of multiple orientations randomly distributed on the surface.

An interesting discovery was made after storing these samples at room temperature in air for 3 months. The h-BN films on Cu foil, Cu (110) and Cu (100) exhibited a shift in the A_{2u}(LO) peak toward higher energy and became more narrow, while the spectrum for the film on Cu (111) did not change (Fig. 8b). XPS spectra (not shown) verified the presence of copper oxide in the samples that exhibited the peak shift. After this observation, all four samples were annealed at 500 °C under a flow of 180 sccm of N_2 and 20 sccm of H_2 for 1 hour. The FT-IRRAS data recorded after annealing are shown in Fig. 8c. As a result of annealing after storage, the A_{2u}(LO) bands of all samples shifted toward lower energies. The whole cycle of evolution of the h-BN A_{2u}(LO) peaks after growth, following storage and annealing, is shown using the Cu foil sample in Fig. 8d as an illustration of the observed behavior pattern of the spectra.

Combining the experimental and computational results discussed above leads to a reasonable explanation for the existence of two A_{2u}(LO) phonon peaks as an effect of coupling between the 2D h-BN and the substrate. In the growth experiment with Cu (111), (110), (100) and foil samples the 2D h-BN is coupled to varying degrees with the substrate as indicated by the position of the A_{2u}(LO)1 band, and it has the strongest interaction with the Cu (111) surface. Accordingly, the peak of the A_{2u}(LO)1 vibration on Cu (111) exhibits the biggest red shift relative to bulk h-BN. The observed shift of this peak toward lower energy following the order from (110) < (100) < (111) could be attributed to the change of the atomic density of each surface orientation following the same order from the lowest density for (110) to the highest density for (111).[38] The more Cu atoms on the surface the stronger the interaction between h-BN and Cu is expected to be. From the perspective of the spectral evolution, during three months of storage the Cu underlying a discontinuous film of h-BN oxidizes, leading to decoupling of the film from the substrate. This results in a blue shift of the A_{2u}(LO)1 band toward the 824 cm^{-1} position of the A_{2u}(LO)2 band (Fig. 8b). At the same time the peaks became narrower because the decoupled h-BN lattice is less distorted than one that is interacting with the Cu surface. This is illustrated by the results in Table 2, which show that the buckling of an h-BN monolayer (as reflected in N_Z–B_Z) increases with the strength of the interaction with the substrate. Only the Cu (111) sample failed to show this shift, which means that the Cu most likely did not oxidize underneath h-BN on Cu (111). This suggests that the stronger bonding between Cu (111) and h-BN, along with the formation of a more continuous film, inhibits oxidation. Annealing in an H_2 atmosphere reduced the Cu oxide, which leads to the red shift in the A_{2u}(LO) vibration demonstrated by all samples (Fig. 8c, d).

Thus, the shift can be explained by the increased h-BN/substrate interaction due to the partial or complete removal of the intermediate oxide layer from the interface. It is, furthermore, possible that the lowest Cu (111) frequency observed here (817.9 cm^{-1}, Fig. 8c) might not represent the absolute limit since the real surface, unlike that in the calculation, is not necessarily atomically smooth, flat and clean. It is noteworthy that others[10,39] have observed a red-shift in the surface-normal mode of h–BN on the (111) surfaces of Ni, Pd and Pt using high-resolution electron energy loss spectroscopy (HREELS). These metals interact more strongly with h-BN than does Cu (111) (ref. 29) and hence exhibit larger shifts. In the case of Ni (111) it was also found that a layer of graphene either on top of the h–BN or between the Ni and the h-BN greatly reduces the interaction and eliminates the shift. These results are entirely consistent with those presented here, but the higher resolution in IRRAS (4 cm^{-1}) *vs.* HREELS (~20 cm^{-1}) has allowed us to analyze small and subtle changes in the relatively-weak h-BN–Cu interaction. This is important in view of the wide-spread use of Cu as a substrate for h-BN growth and the present objective of developing IRRAS as a simple and effective characterization technique. It should also be noted that, as discussed by Berreman,[19] the mode excited in a *p*-polarized, grazing-incidence IRRAS experiment for a thin dielectric layer on a metal substrate appears at the LO frequency of the dielectric and is commonly labeled as such, even though the propagating wave is in fact transverse. In the HREELS data discussed above, the same mode is observed as the dominant loss feature in specular scattering, which is also subject to electric-dipole selection rules, but is conventionally labelled as TO.

Further oxidation testing shown in Fig. 9, revealed the possibility of a more complex impact of oxidation on h-BN films on polycrystalline Cu foils. For spectrum (a) the as-grown h-BN is in essentially uniform contact with the substrate and shows only the red-shifted mode at 819.7 cm^{-1}; whereas, in spectrum (b) for another sample from another run the as-grown h-BN is uniformly decoupled and shows only the unshifted peak at 824.4 cm^{-1}. The growth conditions that result in a coupled or uncoupled hBN film will be published elsewhere with the new understanding based on the results of this paper. After 20 months of storage at RT in air, the former sample shows, in spectrum (a1), that most of the h-BN has become decoupled from the substrate due to oxidation resulting in the appearance of a second peak at 823.5 cm^{-1}. On the other hand the latter sample shows, in spectrum (b1), no effect since the h-BN was already decoupled from the substrate.

To show the validity of the applied technique as well as to verify the model and data interpretation described above, two h-BN samples – one on Cu foil and another on polycrystalline Ni were grown in the same run. The resulting FT-IRRAS data are shown in Fig. 10 and are in good agreement with the

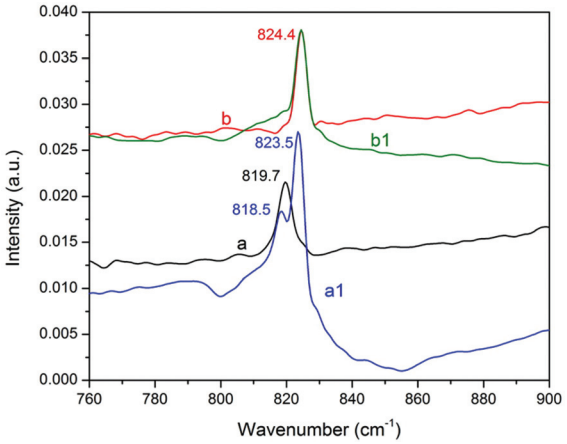

Fig. 9 FT-IRRAS for h-BN on copper foils before (spectra a and b) and after 20 months storage in air (spectra a1 and b1). The 819.7 cm^{-1} band of samp le "a" splits into two bands, at 818.5 cm^{-1} and 823.5 cm^{-1} (a1), indicating decoupling of some of the h-BN from the substrate due to Cu oxidation. The 824.4 cm^{-1} band of the sample "b" indicates an h-BN layer that is already decoupled from the substrate and is thus unaffected (b1) by Cu oxidation.

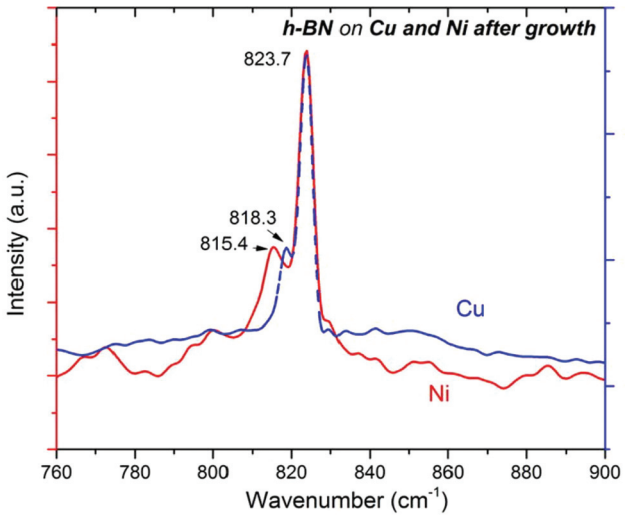

Fig. 10 FT-IRRAS data for h-BN grown in the same nm on a polycrystalline Ni substrate and on Cu foil. 2D h-BN has a stronger interaction with Ni than with Cu, which results in larger red shift of A_{2u}(LO)1 band. Peaks of A_{2u}(LO)2 band related to uncoupled h-BN are at the same position for both samples.

suggested interpretation for the behavior of the A_{2u}(LO) band. Both samples exhibit both A_{2u}(LO)1 and A_{2u}(LO)2 bands. The lower-energy A_{2u}(LO)1 band is related to areas of h-BN coupled with substrate, while the higher-energy A_{2u}(LO)2 band appears at exactly the same energy for both substrates. The interaction between an h-BN film and Ni (111) is known[11,29] to be much stronger than that with Cu (111). This is reflected in the observed larger red shift of the A_{2u}(LO)1 band for the Ni sample when compared with the Cu sample (Fig. 10). At the same time both Ni and Cu samples have the same A_{2u}(LO)2 bands attributed to decoupled 2D h-BN with the peak at 823.7 cm^{-1}. One further observation confirms the interpretation of the A_{2u}(LO) band shift presented here. All thick h-BN samples, like Sample #6 shown in Fig. 6, demonstrated a dominant or single A_{2u}(LO)2 mode around 824 cm^{-1}. Given the understanding of the influence of coupling between h-BN and substrate on A_{2u}(LO), this is expected because of the major contribution of h-BN layers distant from the Cu surface. Basically such multilayer systems exhibit two states. One state pertains to the layer in direct contact with the substrate and the other state to all higher-lying layers.

Conclusion

In conclusion, FT-IRRAS data have been used to characterize monolayer and few-layer h-BN films directly on metal substrates. Two sub-bands of the A_{2u}(LO) vibrational mode were, for the first time, found for thin 2D h-BN films in contact with Cu and Ni. To unveil the nature of the discovered sub-bands, *ab-initio* calculations were performed and verified using 2D h-BN films grown on various Cu substrates with varying coverages and with individual crystallites of different shapes and size up to 4 μm. It was shown that the lower-energy A_{2u}(LO)1 sub-band around 819 cm^{-1} is related to 2D h-BN coupled with Cu substrate, while the higher energy A_{2u}(LO)2 sub-band around 824 cm^{-1} is related to decoupled (essentially free standing) 2D h-BN. These findings demonstrate not only a new and facile method for immediate 2D h-BN identification and characterization, but also a method that provides a simple means to characterize the degree of coupling between 2D h-BN and the substrate. This approach also provides an opportunity to determine which growth conditions lead to the absorption of foreign species on the substrate prior to the h-BN deposition and which conditions can prevent the formation of the interfacial layer between h-BN and the substrate. Such interfacial layers, like oxidized Cu, were shown to result in easily-recognizable shifts in the A_{2u}(LO) peak. The degree to which the interaction of the h-BN layer with the substrate is uniform and homogenous can also be assessed easily by examining the width and fine structure of the A_{2u}(LO) band. The developed approach can also be used to study growth and formation of h-BN/graphene and other 2D heterostructures.

Acknowledgements

The authors gratefully acknowledge the Naval Research Laboratory basic research program and the Office of Naval Research for support of this work. Authors also gratefully acknowledge Dr Kurt Gaskill and Dr Fritz Kub for their support of this work. Also, Z.R.R. would like to thank the American Society for Engineering Education for his postdoctoral support.

References

1 K. S. Novoselov, D. Jiang, F. Schedin, T. J. Booth, V. V. Khotkevich, S. V. Morozov and A. K. Geim, *Proc. Natl. Acad. Sci. U. S. A.*, 2005, **102**, 10451–10453.

2 C. R. Dean, A. F. Young, I. Meric, C. Lee, L. Wang, S. Sorgenfrei, K. Watanabe, T. Taniguchi, P. Kim, K. L. Shepard and J. Hone, *Nat. Nanotechnol.*, 2010, **5**, 722–726.

3 W. Gannett, W. Regan, K. Watanabe, T. Taniguchi, M. F. Crommie and A. Zettl, *Appl. Phys. Lett.*, 2011, **98**, 242105.

4 M. Jansen, R. Haubner, M. Wilhelm, R. Weissenbacher and B. Lux, in *High Performance Non-Oxide Ceramics II*, Springer, Berlin, Heidelberg, 2002, vol. 102, pp. 1–45.

5 K. Watanabe, T. Taniguchi and H. Kanda, *Nat. Mater.*, 2004, **3**, 404–409.

6 E. K. Sichel, R. E. Miller, M. S. Abrahams and C. J. Buiocchi, *Phys. Rev. B: Solid State*, 1976, **13**, 4607–4611.

7 I. Jo, M. T. Pettes, J. Kim, K. Watanabe, T. Taniguchi, Z. Yao and L. Shi, *Nano Lett.*, 2013, **13**, 550–554.

8 L. Britnell, R. V. Gorbachev, R. Jalil, B. D. Belle, F. Schedin, A. Mishchenko, T. Georgiou, M. I. Katsnelson, L. Eaves, S. V. Morozov, N. M. R. Peres, J. Leist, A. K. Geim, K. S. Novoselov and L. A. Ponomarenko, *Science*, 2012, **335**, 947–950.

9 K. S. Novoselov, V. I. Falko, L. Colombo, P. R. Gellert, M. G. Schwab and K. Kim, *Nature*, 2012, **490**, 192–200.

10 E. Rokuta, Y. Hasegawa, K. Suzuki, Y. Gamou, C. Oshima and A. Nagashima, *Phys. Rev. Lett.*, 1997, **79**, 4609–4612.

11 A. B. Preobrajenski, A. S. Vinogradov and N. Martensson, *Surf. Sci.*, 2005, **582**, 21–30.

12 L. Song, L. J. Ci, H. Lu, P. B. Sorokin, C. H. Jin, J. Ni, A. G. Kvashnin, D. G. Kvashnin, J. Lou, B. I. Yakobson and P. M. Ajayan, *Nano Lett.*, 2010, **10**, 3209–3215.

13 R. Y. Tay, M. H. Griep, G. Mallick, S. H. Tsang, R. S. Singh, T. Tumlin, E. H. T. Teo and S. P. Karna, *Nano Lett.*, 2014, **14**, 839–846.

14 D. Sánchez-Portal and E. Hernández, *Phys. Rev. B: Condens. Matter*, 2002, **66**, 235415.

15 N. Ohba, K. Miwa, N. Nagasako and A. Fukumoto, *Phys. Rev. B: Condens. Matter*, 2001, **63**, 115207.

16 S. D. Costa, A. Righi, C. Fantini, Y. Hao, C. Magnuson, L. Colombo, R. S. Ruoff and M. A. Pimenta, *Solid State Commun.*, 2012, **152**, 1317–1320.

17 R. V. Gorbachev, I. Riaz, R. R. Nair, R. Jalil, L. Britnell, B. D. Belle, E. W. Hill, K. S. Novoselov, K. Watanabe, T. Taniguchi, A. K. Geim and P. Blake, *Small*, 2011, **7**, 465–468.

18 R. G. Greenler, *J. Chem. Phys.*, 1966, **44**, 310–315.

19 D. W. Berreman, *Phys. Rev.*, 1963, **130**, 2193–2198.

20 P. Giannozzi, S. Baroni, N. Bonini, M. Calandra, R. Car, C. Cavazzoni, D. Ceresoli, G. L. Chiarotti, M. Cococcioni, I. Dabo, A. D. Corso, S. d. Gironcoli, S. Fabris, G. Fratesi, R. Gebauer, U. Gerstmann, C. Gougoussis, A. Kokalj, M. Lazzeri, L. Martin-Samos, N. Marzari, F. Mauri, R. Mazzarello, S. Paolini, A. Pasquarello, L. Paulatto, C. Sbraccia, S. Scandolo, G. Sclauzero, A. P. Seitsonen, A. Smogunov, P. Umari and R. M. Wentzcovitch, *J. Phys.: Condens. Matter*, 2009, **21**, 395502.

21 S. Grimme, *J. Comput. Chem.*, 2006, **27**, 1787–1799.

22 I. Rupsky and I. Iordanova, *Phys. Status Solidi A*, 1991, **127**, 23–32.

23 J. F. Moulder, W. F. Stickle, P. E. Sobol and K. D. Bomben, *Handbook of X-Ray Photoelectron Spectroscopy*, Physical Electronics, Eden Prairie, MN, 1995.

24 Y. Cai, L. Zhang, Q. Zeng, L. Cheng and Y. Xu, *Solid State Commun.*, 2007, **141**, 262–266.

25 C. S. Fadley, Basic Concepts of X-Ray Photoelectron Spectroscopy, in *Electron Spectroscopy: Theory, Techniques and Applications*, ed. C. R. Brundle and A. D. Baker, Academic Press Inc., 1978, vol. 2.

26 B. R. Strohmeier, *Surf. Interface Anal.*, 1990, **15**, 51–56.

27 J. H. Scofield, *J. Electron Spectrosc. Relat. Phenom.*, 1976, **8**, 129–137.

28 C. J. Powell and A. Jablonski, NIST Electron Effective-Attenuation-Length Database, Vers. 1.3, *U.S. Department of Commerce*, National Institute of Standards and Technology, Gaithersburg, MD, 2011, SRD 82.

29 R. Laskowski, P. Blaha and K. Schwarz, *Phys. Rev. B: Condens. Matter*, 2008, **78**, 045409.

30 R. Koitz, A. P. Seitsonen, M. Iannuzzi and J. Hutter, *Nanoscale*, 2013, **5**, 5589–5595.

31 J. Gómez Díaz, Y. Ding, R. Koitz, A. Seitsonen, M. Iannuzzi and J. Hutter, *Theor. Chem. Acc.*, 2013, **132**, 1–17.

32 Y. Li and R. Mazzarello, *Phys. Rev. B: Condens. Matter*, 2013, **88**, 045317.

33 G. I. Csonka, J. P. Perdew, A. Ruzsinszky, P. H. T. Philipsen, S. Lebègue, J. Paier, O. A. Vydrov and J. G. Ángyán, *Phys. Rev. B: Condens. Matter*, 2009, **79**, 155107.

34 W. Paszkowicz, J. Pelka, M. Knapp, T. Szyszko and S. Podsiadlo, *Appl. Phys. A*, 2002, **75**, 431–435.

35 M. Halo, C. Pisani, L. Maschio, S. Casassa, M. Schütz and D. Usvyat, *Phys. Rev. B: Condens. Matter*, 2011, **83**, 035117.

36 K. Doll and N. M. Harrison, *Chem. Phys. Lett.*, 2000, **317**, 282–289.

37 S. Joshi, D. Ecija, R. Koitz, M. Iannuzzi, A. P. Seitsonen, J. Hutter, H. Sachdev, S. Vijayaraghavan, F. Bischoff, K. Seufert, J. V. Barth and W. Auwärter, *Nano Lett.*, 2012, **12**, 5821–5828.

38 Z. R. Robinson, P. Tyagi, T. M. Murray, C. A. Ventrice, S. Chen, A. Munson, C. W. Magnuson and R. S. Ruoff, *J. Vac. Sci. Technol., A*, 2012, **30**, 011401–011407.

39 C. Oshima, A. Itoh, E. Rokuta, T. Tanaka, K. Yamashita and T. Sakurai, *Solid State Commun.*, 2000, **116**, 37–40.

